2025 IEEE/SICE International Symposium on System Integration (SII)
January 21-24, 2025, Munich, Germany

Artificial Finger Consisting of Closed Linkages and a Single Planetary Gear System: Control of a Reaction Force Vector Yielded at a Fingertip

Y. Eto, K. Koganezawa, and Y. Kai

Abstract—**The authors have developed a five-finger robot hand with artificial fingers consisting of closed linkages and a Single Planetary Gear System. Recently, we developed a new finger mechanism equipping a hyperextension joint at the fingertip that acts passively by two torsion springs. This paper aims to investigate how the hyperextension joint allows to control the reaction force vector that the fingertip applies to an external object in kinematic & kinetic theoretical point of view.**

I. Introduction

We have developed a five-finger robot hand aiming for applying as artificial or prosthetic hands [1]-[6]. Especially, we have considered three necessary points that the new hand should have in a perspective of practical usage. It should have *robustness* in consideration of using it in harsh environments, *variable joint stiffness* to bring in flexible motions, and allowing *envelope grasping* of shape-uncertain objects. Why do we focus on these functions? Because of that past studies on artificial hands have not been enough to fulfill them[7][8]. For example, the famous robot hand "Gifu hand" achieves sophisticated motions with a lot of actuators, but it lacks robustness against harsh environments [9]. Widely used Ottobock prosthetic hand has an elegant appearance and is useful as a hand-prosthesis. But it lacks sufficient degree-of freedom (DOF) enough to cover the necessary functions a human hand has [10].

In our hand developed so far, four fingers (index, mid, medicinal, and little) have a common mechanism, two serially connected closed four-bar linkages, and a Single Planetary Gear System (SPGS). This finger mechanism is driven by active sun gear rotation and passive pre-tension of the carrier rotation. It constitutes a 2-DOF mechanical system that drives as active and passive amalgamation. This mechanism roles as a *variable stiffness mechanism* (VSM). The VSM achieves a sensorless shape-fitting motion (envelope grasping) for uncertain shape or weight objects. Moreover, it has robustness in harsh environments usage because no electric or electronic devices are embedded in the finger part. Details of the mechanisms are shown in Chap. 3. Chap.4 derives the theoretical formulation. Chap.5 describes the simulation study followed in conclusions.

II. Research Purpose

We found that the finger mechanism without a hyperextension joint, our previously developed finger, has a problem. Under the fingertip contact with an external object, the sun gear rotation is unable to change the fingertip reaction force vector while holding the fixed contact position in the Cartesian coordinate system. Although, it allows to pinch objects and lift them up by two fingers, its motion sometimes revealed being unstable, because of which is a lack of controllability of pinching force.

To resolve this problem, we developed a new finger mechanism having a Hyperextension DIP joint (H-joint, hereafter). This mechanism provides a passive degree of freedom at the DIP joint. It also aims for making stabilized pinching motions in a passive manner by springs equipped in the mechanism. Therefore, we need to verify how the fingertip force of the new finger mechanism is changed with the spring coefficient or its pre-tension. This is the research purpose.

In this paper, we expect 2 items to be derived through simulation studies.

(1) How the linkage mechanism and elastic elements interact from kinematic and kinetic points of view in constructing their formulation.

(2) How the hyperextension joint affects the pinch motion, especially for regulating the pinching force vector.

If a new finger mechanism provides a function of regulating the fingertip force vector, we think it can stabilize the sensorless pinching motion.

In one previous study, the finger mechanism is passively changeable joint stiffness only at the DIP joint [11]. However, it is not a closed linkage mechanism and has no passive mechanism in the MP joint for envelope grasping. In addition, there also have been finger mechanism studies that extend passively.[12][13] However, MP, PIP, and DIP joints in the finger mechanism in those studies are monotonically moving together. Therefore, it is not possible to extend the DIP joint only.

On the other hand, our finger mechanism is changeable joint stiffness including MP and PIP joints. Consequently, we consider that our finger mechanism is more suitable for sensorless shape-fitting motions (envelope grasping) for uncertain shape or weight objects.

Y. Eto is with Ph.D Course, Graduate School of Science and Technology Tokai University, 4-1-1 Kitakaname, 259-1292, Hiratsuka, Japan, (3ctad003@cc.u-tokai.ac.jp)

K. Koganezawa is with Tokai University, (kogane@tokai.ac.jp)

Y. Kai is with the Department of Mechanical Systems Engineering, Tokai University, (kai@tokai.ac.jp)

III. MECHANISM

A. *Finger Mechanism*

Fig. 1 shows the finger mechanism with a newly employed hyperextension joint. The solar gear is driven actively by a DC-motor and the pre-tension of the carrier is adjusted by another DC-motor. All electric or electronic devices are embedded in the parm part for providing robustness in taking into consideration of harsh environments usage. The finger mechanism enables shape-fitting motion with various shapes of objects as a VSM. The length of the finger links and inner gear in the planetary gear mechanism are determined based on anatomical data [14][15]. In addition, it is designed to decrease the extra bulging shape in linkage mechanisms. In Fig. 2, we show the average thickness of each joint in the average adult Japanese.

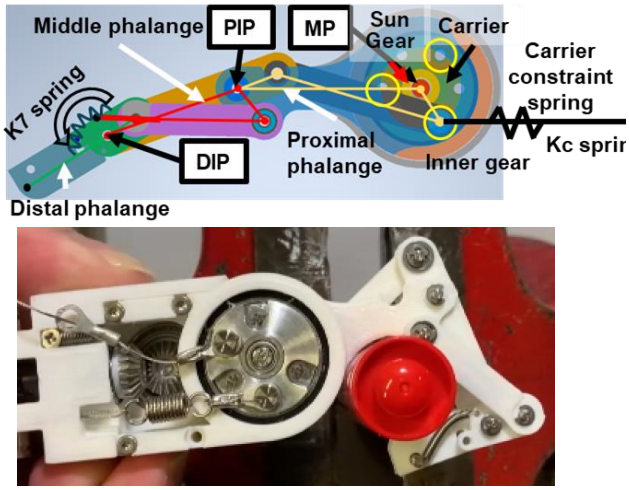

Figure 1. Finger mechanism

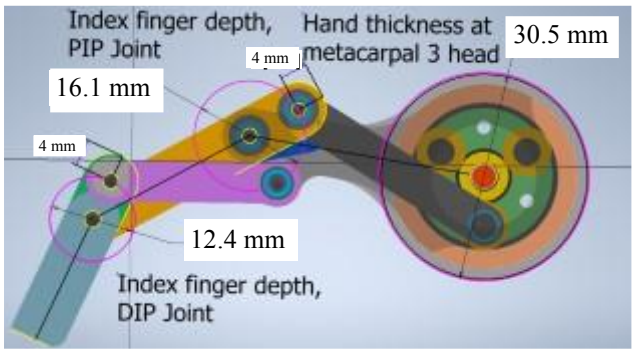

Figure 2 finger size

B. *Hyperextension joint (H-joint)*

Fig. 3 shows the H-joint. Hyperextension at the distal phalanx joint provides passive warping with two torsion springs. It aims to stabilize pinching motions passively as same as human fingers.

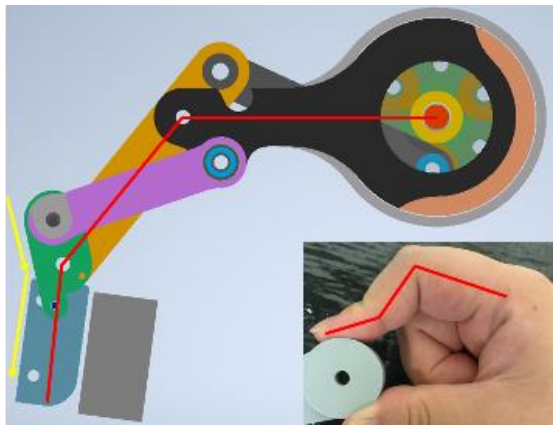

Figure 3. Hyperextension mechanism

C. *Variable Stiffness Mechanism (VSM)*

Fig. 4 shows the overview of the VSM. Under no external force loading at the finger, the tension between spring 1 and spring 2 is statically balanced. The constrain of carrier rotation due to the tension of the spring 2 by the rotation of the wire shaft by the motor (VSM motor, hereafter) provides a torque to the finger mechanism. This is two degrees of freedom (2-DOF) system driven actively by the sun-gear rotation by a motor and passively by the carrier rotation with a spring, but of which pre-tension can be adjusted by the VSM motor.

Thus, this finger is composed of mechanical elements, yet allows for flexible grasping, notably, envelope grasping of uncertain-shape objects as shown in Fig.4

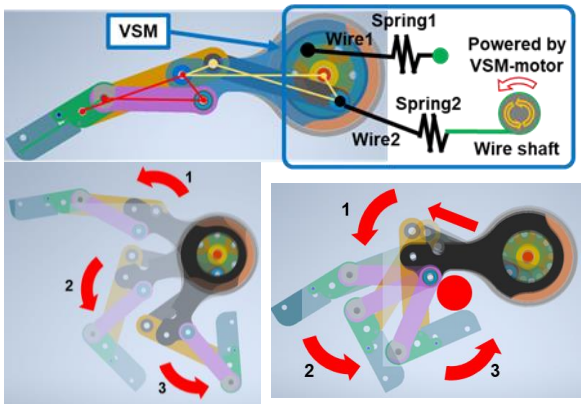

VSM : High VSM: Low

Figure 4. VSM

IV. SIMULATION: KINETIC & KINEMATIC FORMULATION

We proceed with a simulation study under the assumptions as follows:

(1) [Drive input] Sun gear rotation angle θs is constantly decreased. (In this simulation, counterclockwise is plus.)

(2) Fingertip position is prescribed as $\boldsymbol{P_T} = P_{Tr} + iP_{Ti}$ and must be sustained (no sliding action is occurred).

(3) This is a simulation in a static situation, holding kinematic and kinetic balance.

(4) No gravitational effect is considered because all of the finger parts are made of light material.

A. Simulation Process

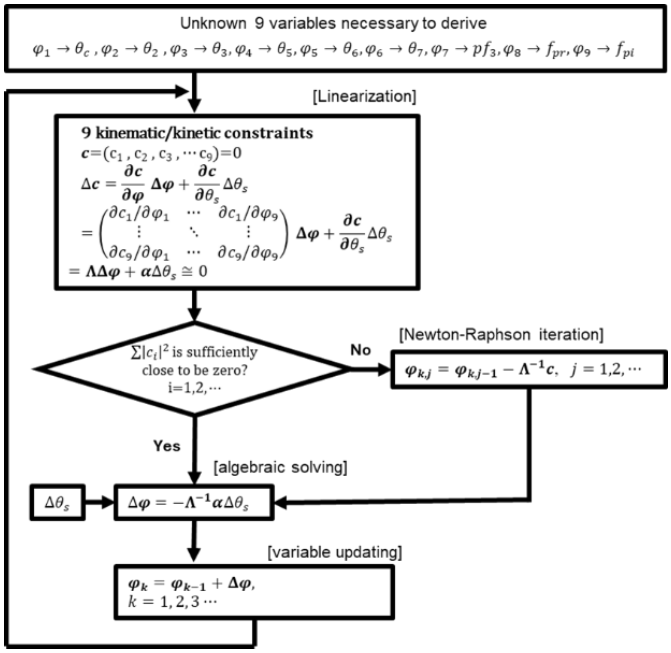

Figure 5. Simulation process

We compute variations of internal nine variables (θ_c, θ_2, θ_3, θ_5, θ_6, θ_7, f_3, fpr, and fpi) by repeatedly updating nine variables in the linearized equations so as to be sustaining kinetic/kinematic nine constraint equations. Details of simulation methods are shown in Chapter 4-B.

Fig. 5 is a flow chart of the simulation process and method. Fig.6 shows the configuration of the joints on a planar surface. Table 1. shows the initial values for the simulation. They are the same lengths as actual equipment linkages.

TABLE I. INITIAL PARAMETERS

Initial Parameters			
φ	50 deg	l_{12}	7.2 mm
θ_c	90 deg	l_{14}	34.6 mm
θ_1	-10 deg	l_{23}	31.9 mm
θ_2	-120 deg	l_{34}	8.05 mm
θ_3	65 deg	l_{45}	8.05 mm
θ_5	-118 deg	l_{47}	25.9 mm
θ_6	70 deg	l_{56}	24.2 mm
θ_7	0 deg	l_{67}	6.2 mm
pf_3	0 N	l_{78}	19.5 mm
f_{pr}	0 N		
f_{pi}	0 N		

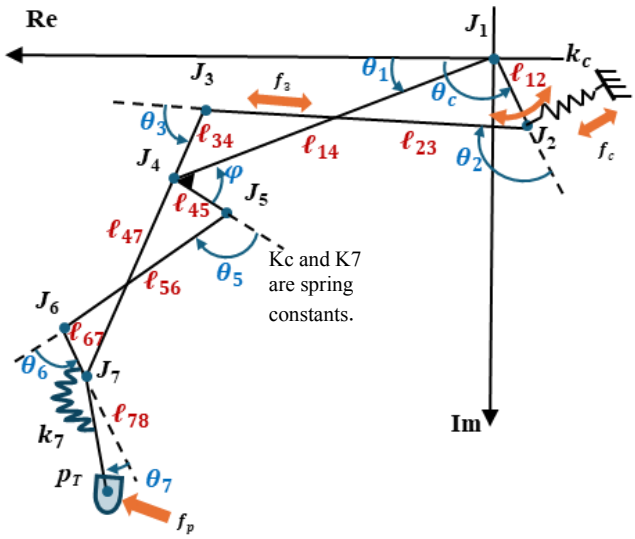

θ_s : Rotation angle of the sun gear.

θ_c : Rotation angle of the carrier that is passively determined by an external load.

$\theta_2 \cdots \theta_5$: Dependent angles that are passively determined by kinematic constraints and kinetic constraints.

$$\theta_1 = \frac{-Z_s}{Z_i}\theta_s + \frac{Z_s+Z_i}{Z_i}\theta_c$$

Z_s=tooth number of the sun gear, Z_i=tooth number of the inner gear

φ : A constant degree.

P_T : The tip position being prescribed.

$$\boldsymbol{P}_T = P_{Tr} + iP_{Ti}$$

f_p : The tip force vector

$$\boldsymbol{f}_p = f_{pr} + if_{pi}$$

Figure 6. Kinematic representation of the finger with hyperextension joint.

B. Constraint equations and simulation method

• Constraint equations 1~4:

In this mechanism, $\boldsymbol{J_4}$ and $\boldsymbol{J_7}$ have two passes to reach their positions due to closed linkages. It gives us the first through fourth kinematic constraint equations.

$$c_1 + ic_2 = (l_{14}e^{i\theta_1}) - (\boldsymbol{J_3} + l_{34}e^{i(\theta_c+\theta_2+\theta_3)}) = 0 + i\times\boldsymbol{0} \quad (1)$$

$$c_3 + ic_4 = (\boldsymbol{J_4} + l_{47}e^{i(\theta_c+\theta_2+\theta_3)}) - (\boldsymbol{J_6} + l_{67}e^{i(\theta_1+\pi-\varphi+\theta_5+\theta_6)}) = 0 + i\times\boldsymbol{0} \quad (2)$$

• Constraint equations 5:

The sum of the force vectors acting at the $\boldsymbol{J_2}$ must be in parallel to the vector $\boldsymbol{J_2}-\boldsymbol{J_1}$, on an equilibrium state, which provides a constraint described by outer product of $\boldsymbol{f_3}+\boldsymbol{f_c}$, and $\boldsymbol{J_2}-\boldsymbol{J_1}$, being zero.

$$c_5 = (\boldsymbol{f_3}+\boldsymbol{f_c})\times(\boldsymbol{J_2}-\boldsymbol{J_1}) = 0 \quad (3)$$

$\boldsymbol{f_3}$ is the internal force vector acting on the link $\boldsymbol{J_2}-\boldsymbol{J_1}$, $\boldsymbol{f_c}$ is a carrier spring force vector, and it has the initial compression force. The operator "×" is defined as $\boldsymbol{p}\times\boldsymbol{q} = p_r q_i - p_i q_r$, for $\boldsymbol{p} = p_r + \boldsymbol{i}p_i$, and $\boldsymbol{q} = q_r + \boldsymbol{i}q_i$, because of dealing with a planar surface motion.

• Constraint equations 6:

The sum of the torque, T_7+T_p, acting at the $\boldsymbol{P_T}$ is zero in a static situation

$$c_6=\boldsymbol{T_7}+\boldsymbol{T_p}=0 \quad (4)$$

$\boldsymbol{T_7}$ is a torque generated by the torsion springs at $\boldsymbol{J_7}$, and T_p is a torque generated by reaction force at the fingertip.

• Constraint equations 7:

The torque acting at $\boldsymbol{J_4}$ is zero in an equilibrium state.

$$c_7=\boldsymbol{f_3}\times(\boldsymbol{J_4}-\boldsymbol{J_3})+\boldsymbol{f_p}\times(\boldsymbol{J_4}-\boldsymbol{P_T})=0 \quad (5)$$

• Constraint equations 8 and 9:

The fingertip position is prescribed as $\hat{\boldsymbol{P}}_{\mathbf{T}}=\hat{\boldsymbol{P}}_{\mathbf{Tr}}+i\hat{\boldsymbol{P}}_{\mathbf{Ti}}$, and must be maintained.

$$c_8+ic_9=\hat{P}_{Tr}+i\hat{P}_{Ti}-\left(\boldsymbol{J_6}+l_{67}e^{i(\theta_1+\pi-\varphi+\theta_5+\theta_6+\theta_7)}\right)=0+i\times\mathbf{0} \quad (6)$$

Resultingly the mechanism possesses a set of infinitesimal variations of nine constraint equations that should hold zero vectors during motion.

$$\Delta\mathbf{c}=(\Delta c1\ \Delta c2\ \Delta c3\ \Delta c4\ \Delta c5\ \Delta c6\ \Delta c7\ \Delta c8\ \Delta c9)=\mathbf{0}_9 \quad (7)$$

From here, we show the details of our simulation method. Before calculating, we denote the variables to be solved as the following:

$$\varphi_1\rightarrow\theta_s,\ \varphi_2\rightarrow\theta_c,\ \varphi_3\rightarrow\theta_1,\ \varphi_4\rightarrow\theta_2,\ \varphi_5\rightarrow\theta_3,\ \varphi_6\rightarrow\theta_4,\ \varphi_7\rightarrow f_{pr},\ \varphi_8\rightarrow f_{pi} \quad (8)$$

At first, we need to take the total differentiation of all constraint equations to compose a matrix equation, as shown in Eq. (9).

$$\Delta\mathbf{c}=\frac{\partial\mathbf{c}}{\partial\boldsymbol{\varphi}}\Delta\boldsymbol{\varphi}+\frac{\partial\mathbf{c}}{\partial\theta_s}\Delta\theta_s=\begin{pmatrix}\partial c_1/\partial\varphi_1 & \cdots & \partial c_1/\partial\varphi_9\\ \vdots & \ddots & \vdots\\ \partial c_9/\partial\varphi_1 & \cdots & \partial c_9/\partial\varphi_9\end{pmatrix}\Delta\boldsymbol{\varphi}+\frac{\partial\mathbf{c}}{\partial\theta_s}\Delta\theta_s$$
$$=\boldsymbol{\Lambda}\Delta\boldsymbol{\varphi}+\boldsymbol{\alpha}\Delta\theta_s\cong\mathbf{0} \quad (9)$$

Eq. (9) gives us a solution of infinitesimal dependent vector $\Delta\boldsymbol{\varphi}$, as shown in Eq. (10).

$$\Delta\boldsymbol{\varphi}=-\boldsymbol{\Lambda}^{-1}\boldsymbol{\alpha}\Delta\theta_s \quad (10)$$

Repeatedly updating $\boldsymbol{\varphi}=(\varphi_1,\ \varphi_2,\varphi_3,\ \varphi_4,\ \varphi_5,\ \varphi_6,\ \varphi_7,\ \varphi_8,\ \varphi_9)^T$ is achieved by adding $\Delta\boldsymbol{\varphi}$ to the previous $\boldsymbol{\varphi}$.

$$\boldsymbol{\varphi}_k=\boldsymbol{\varphi}_{k-1}+\Delta\boldsymbol{\varphi}\ ,\ k=1,2,3\cdots \quad (11)$$

The numerical errors generated by the linear approximation will be compensated by employing the Newton-Raphson convergency procedure in the cycle (see Fig. 5).

$$\boldsymbol{\varphi}_{k,j}=\boldsymbol{\varphi}_{k,j-1}-\boldsymbol{\Lambda}^{-1}\mathbf{c},\ j=1,2,\cdots, \quad (12)$$

where k and j are an iteration number and $\varphi_{k,0}=\varphi_k$.

V. Simulation: Result

First, we show the simulation results in the case of the hyperextension joint being absent to show the necessity of the H-joints. Next, we show the simulation results of three different situations. Finally, we present our conclusions derived from these simulation results.

A. Simulation 1: The case of the *H-joint assumed not to be incorporated*

In this section, we show the case of the finger mechanism without the H-joint. As noted above, the finger mechanism without the H-joint is unable to regulate the contact force vector due to a lack of DOF, especially its direction while holding the contact position under the fingertip contacting with an external object. Therefore, in this simulation, we show a case that the fingertip position is free on the horizontal axis direction. We omit the constraint equation 8 as well as the unknown variables θ7 and a slight friction force is assumed to be yielded during horizontal sliding as *fpr* (the horizontal component of $\boldsymbol{f_P}$).

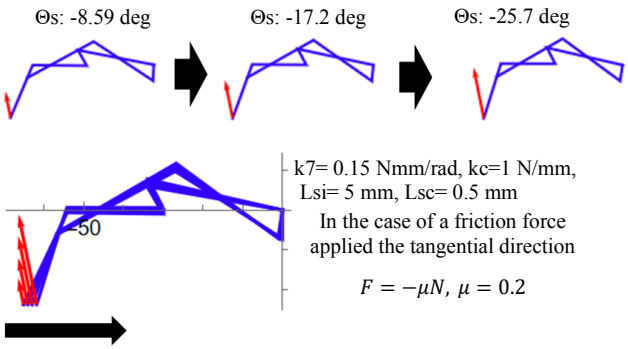

Figure 7. Simulation results: no hyperextension joint

Fig. 7 shows reaction forces with red arrows while the fingertip traces a horizontal surface. The reason the red arrows being slanted a little is due to a friction force assumed to be yielded on the tracing surface. As shown in Fig. 7, the magnitude of the reaction force is determined by the finger posture. As a characteristic of the previously developed finger mechanism, the H-joint offers one more DOF for regulating the fingertip force vector under the fingertip position being fixed.

B. Simulation 2: When the spring constant of kc is changed

We proceed with the simulation study to obtain a clue for selecting the carrier liner spring KC. We examine how the fingertip reaction force vector is changed according to the carrier liner spring KC being varied under the spring coefficient k7 [Nmm/rad] of the fingertip torsion spring being fixed. The carrier spring KC has a spring coefficient kc [N/mm] with a common natural length Lsi [mm]. In addition, the KC has an initial compression length Lsc[mm] that is controllable by the VSM motor. Also, the initial posture of the finger is identical during this simulation.

In this situation, we observed how the value of the spring coefficient kc affects the fingertip reaction force vector. Fig.8 shows the simulation results. There are the results as θs decreases from zero to -26.1 deg.

From the simulation, we found that the trend of the reaction force vector can be classified into three modes according to the value of kc.

(1) Mode A [kc < 0.4]: pushing forward mode.

(2) Mode B [0.5 < kc < 1.9]: rotating direction mode

(3) Mode C [2 < kc]: pushing upward mode

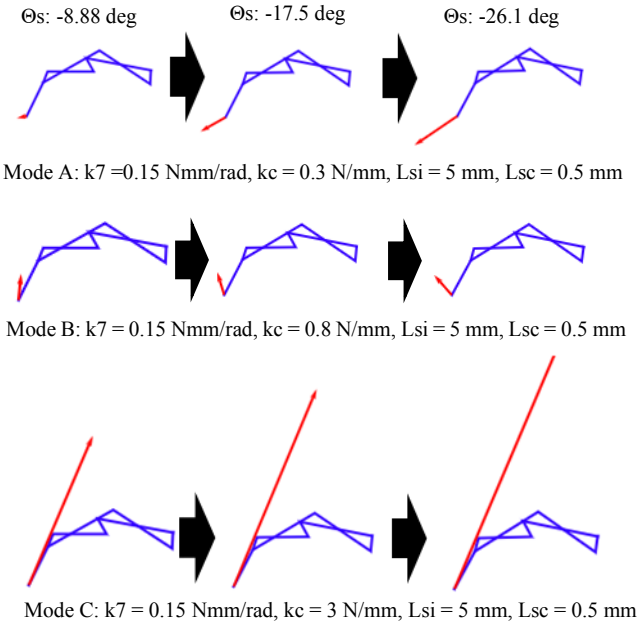

Figure 8. The spring constant of kc being changed

The simulation results show that Mode B provides the fingertip reaction force vector being changeable in its direction by adjusting the solar gear angle θs. On the other hand, Modes A and C have changed the magnitude of the reaction force vector, while the direction changes a little. These results suggest that θs is incapable of adjusting the reaction force vector in its direction while holding the fingertip position during contact with the grasping object if we choose Modes A or C. In conclusion, Mode B is a better choice for the spring coefficient range of KC.

C. Simulation 3: When the initial compression length is changed

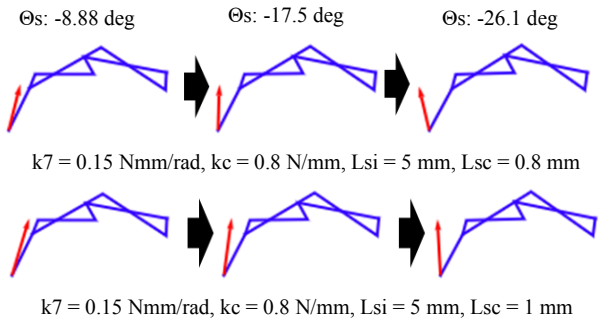

Figure 9. Initial compression lengths are changed

In the actual equipment, the VSM adjusts the initial spring compression Lsc using the VSM motor. Therefore, we observe how the fingertip reaction force vector relates the Lsc. Fig.9 shows the simulation results for the initial compression lengths of 0.8 mm and 1 mm. These simulation results indicate that the initial compression length of the carrier spring allows to change the direction of the reaction force at the fingertip.

D. Simulation 4: When the initial finger posture is changed

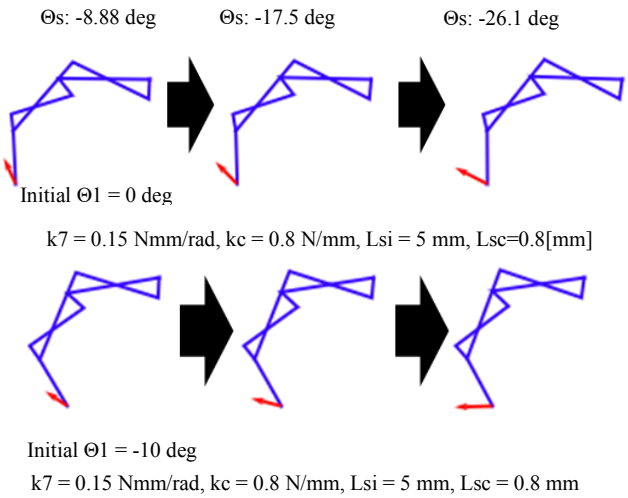

Figure 10. Reaction forces when the initial finger posture is changed

We consider that the shape or size of the grasping object changes the finger posture when it comes into contact with the object. Therefore, we observe the difference in the fingertip reaction force vector on various initial postures of the finger in the simulation. Fig. 10 shows the results of the reaction force vector in three initial finger postures. It is observed that the force direction mainly depends on the finger posture, although its relative direction to the distal link direction is almost the same.

E. Simulation Results' Summary

This section is a summary of the simulation results. First, in the results of Simulation 1, we observe that the hyperextension joint is indispensable to regulating the fingertip force under the fingertip position being fixed in the Cartesian coordinate. Second, the results of Simulations 2 and 3 clearly indicate that the reaction force vector depends on the carrier spring force. In the actual machine, Lsc is adjustable by using the VSM motor to change the spring force strength of the carrier spring KC. Third, the results of Simulation 4 suggest that the direction of the reaction force vector mainly depends on the posture of the finger.

From the above statements, the simulation results elucidate the proposed finger mechanism with the H-joint has prominent properties.

(1) The VSM adjusts the initial tension of the carrier, thereby controlling the fingertip reaction force.

(2) By adjusting the sun-gear angle θs, the direction of the fingertip reaction force vector is controllable.

VI. CONCLUSION

This research purpose was to investigate how the fingertip

force of the new finger mechanism is regulated with spring coefficients or its pre-tension. Especially, we analyzed how the linkage mechanism and springs interacted and proved how the H-joint affects the new finger mechanism by simulation.

First, we analyzed how the linkage mechanism and springs interact kinematically and kinetically. Second, we analytically elucidated that the H-joint is indispensable to regulating the fingertip force vector under the fingertip position being fixed Finally, based on simulation results, we observed that the finger mechanism with the H-joint can control the fingertip reaction force by driving the sun gear and by regulating the pre-tension of the carrier by the VSM motor while the fingertip is in contact with the grasped object.

In our future work, we experimentally verify the simulation results above mentioned. Also, we plan to simulate two-finger pinching to verify the contributions of the H-joint to stabilize the motion.

REFERENCES

[1] Eto. Y, Koganezawa. K, and Kai. Y, "Five-Finger Robot Hand Aimed for a Multi-DOF Prosthetic Hand," Proceedings of the 39th Annual Conference of the Robotics Society of Japan, 3C2-04, September 2023. In Japanese.

[2] Eto. Y, Akiyoshi. K, and Koganezawa. K "Modular Artificial fingers with Variable Stiffness Mechanism using Single & Double Planetary Gear Systems and an application to 3 fingers robot hand," Proceedings of the 7th International Conference on Advanced Mechatronics (ICAM2021), Online (Host Aichi, Japan), July 2021.

[3] Koganezawa. K, Ito, A "Artificial Hand with Stiffness Adjuster," Proceedings of 2014 IEEE International Conference on Intelligent Robots and Systems (IROS), Chicago, USA,2014.

[4] Eto. Y, Koganezawa. K "A Mechanism for Artificial Finger Based on the Double Planetary Gear System -Kinematics and Kinetics Study-," Proceedings of International Symposium on System Integration (SII2022), Narvik, Norway, January 2022.

[5] Y. Eto, K. Koganezawa, Y. Kai, "Artificial finger consisting of closed linkages and Single Planetary Gear System: an approach to grasp stabilizing with a distal hyperextension joint", Proceedings of the 7th International Conference on Multibody System Dynamics (IMSD2024), June 9-13, 2024, Madison, WI, USA.

[6] Y. Eto, K. Koganezawa, Y. Kai, "Artificial Finger Consisting of Closed Linkages and a Single Planetary Gear System: Verification of the Effectiveness of a hyperextension mechanism.", Proceedings of The 42nd annual conference of the Robotics Society of Japan (RSJ2024),

[7] K. Anzawa, H. Sasaki, S. Jeong and T. Takahashi, "Development of a Robot Hand with Low Backlash 3D Cam Mechanisms-Prototype of a Light-weight Robot Hand and Evaluation of the Mechanisms" Journal of the Robotics Society of Japan, Vol.28 No.7 pp.889-896, 2010, in Japanese.

[8] I-Limb Quantum, https://www.ossur.com/en-us/prosthetics/arms/i-limb-quantum, (2024/09/14)

[9] H. Kawasaki, T. Mouri, S. Ito, N. Shimomura, T. Matunami, N. Hanada, T. Azuma, "Anthropomorphic robot hand: Gifu hand III" Journal of the Robotics Society of Japan, Vol.22 No.1 pp.55-56, 2004, in Japanese.

[10] Michelangelo hand, https://www.ottobock.com/ja-jp/prosthetic_ue/myoelectric/axonbus/Michelangelo (2022/08/01)

[11] N. Tani, Y. Jinang, S. Togo, H. Yokoi, "Development of Join Flexion Mechanism with Myoelectric Prosthrtic Hand for Grasp in Power Grasp and Precision Grasp", JRSJ Vol.37 No.2, pp.168-178, 2019, in Japanese.

[12] M. Hioki, S. Ebisawa, H. Sakaeda, T. Mouri, S. Nakagawa, Y.i Uchida, H. Kawasaki, "Design and Control of Electromyogram Prosthetic Hand with High Grasping Force", Proc of. BIOROBO2011, pp.1128-1133, 2011.

[13] N. Dechev, W.L. Cleghorn, S. Naumann, "Multiple finger, passive adaptive grasp prosthetic hand", Mechanism and Machine Theory 36, pp. 1157-1173, 2001

[14] Y. Ueba, Kinpodo Publishers. Inc., "The Hand-its function and anatomy", 6th edition, pp.110, 2017/1/1

[15] M. Kawauchi "AIST Hand length data of Japanese people", https://www.airc.aist.go.jp/dhrt/hand/index.html, 2012